

Bayesian brain mapping: population-informed individualized functional topography and connectivity

Nohelia Da Silva Sanchez, Diego Derman, Damon D. Pham, Ellyn R. Butler, Mary Beth Nebel, Amanda F. Mejia

Abstract

The spatial topography of brain functional organization is increasingly recognized to play an important role in cognition and disease. Accounting for individual differences in functional topography is also crucial for accurately distinguishing spatial and temporal aspects of brain organization. Yet, accurate estimation of individual functional brain networks from functional magnetic resonance imaging (fMRI) without extensive scanning remains challenging, due to low signal-to-noise ratio. Here, we describe Bayesian brain mapping (BBM), a technique for individual functional topography and connectivity leveraging population information. Population-derived priors for both spatial topography and functional connectivity based on existing spatial templates, such as parcellations or continuous network maps, are used to guide subject-level estimation and combat noise. BBM is highly flexible, avoiding strong spatial or temporal constraints and allowing for overlap between networks and heterogeneous patterns of engagement. Unlike multi-subject hierarchical models, BBM is designed for single-subject analysis, making it highly computationally efficient and translatable to clinical settings. Here, we describe the BBM model and illustrate the use of the BayesBrainMap R package to construct population-derived priors, fit the model, and perform inference to identify engagements. A demo is provided in an accompanying Github repo. We also share priors derived from the Human Connectome Project database and provide code to support the construction of priors from different data sources, lowering the barrier to adoption of BBM for studies of individual brain organization.

1 Introduction

The functional organization of the brain is highly individualized, both in terms of the spatial configuration (Gordon et al., 2017) and temporal dynamics (Finn et al., 2015) of functional

brain networks. Individual features of functional topography have been shown to be predictive of various phenotypes, as well as disease severity (Bijsterbosch et al., 2018; Kong et al., 2019; Bijsterbosch et al., 2019; Li et al., 2022). Therefore, functional topography is a potentially valuable source of imaging-based biomarkers for disease diagnosis and treatment efficacy.

Extracting functional topography accurately at the individual level has historically relied on collecting hours of resting-state functional magnetic resonance imaging (fMRI) on individuals (Braga and Buckner, 2017; Gordon et al., 2017; Xue et al., 2021). These “precision neuroimaging” studies have been crucial in establishing the existence of individual differences in spatial topography. However, translational goals, such as the use of functional topography and connectivity features in biomarkers and for personalized treatment, are contingent upon being able to extract these features accurately using moderate amounts of data feasible to collect in clinical settings.

Another motivation for extracting individual function topography from standard-duration scans is its relevance to measurement of functional connectivity (FC), i.e. the temporal synchrony between regions of the brain. The use of group parcellations or network maps misaligned to the individual’s functional topography can lead to biased FC estimates (Smith et al., 2011; Bijsterbosch et al., 2018, 2019) due to mixing of signals from distinct but proximal functional areas. Thus, true differences in functional topography can be misinterpreted as differences in FC. A potential ramification is that real relationships between behavioral or phenotypic measures and functional topography may be incorrectly attributed to FC. If prediction is our main objective, this mixing of features may not be highly consequential. But if we aim to understand the brain mechanisms underlying certain behaviors or disease states, rather than simply predict them, it is crucial to disentangle differences in spatial topography from differences in temporal engagement and connectivity (Harrison et al., 2020).

To extract individual functional topography from typical duration subject-level fMRI data, hierarchical Bayesian models have proven an effective approach. These models reduce noise by combining information from multiple subjects, while respecting individual differences and ensuring correspondence between individuals. Hierarchical models been successfully applied in the context of parcellation (Kong et al., 2019, 2021), probabilistic functional modes (PROFUMO)

(Harrison et al., 2015; Farahibozorg et al., 2021), and independent component analysis (ICA) (Guo and Tang, 2013; Mejia et al., 2020). Importantly, these methods have been shown to perform well based on a modest amount of data per individual, potentially avoiding the need to collect prolonged or repeated sessions of data in individuals. This makes them highly attractive in contexts where extensive subject-level scanning is not feasible, including clinical settings where it presents a financial and physical burden for patients.

In addition to the importance of accounting for individual functional topography, there is growing evidence for the existence and relevance of overlapping functional architecture (Faskowitz et al., 2020). This favors "soft" parcellations allowing for overlap between functional networks over traditional "hard" parcellations (Bijsterbosch et al., 2023; Dadi et al., 2020; Li et al., 2018). Examples of soft parcellation approaches include spatial ICA (Beckmann and Smith, 2004), temporal ICA (Smith et al., 2012), PROFUMO (Harrison et al., 2015), non-negative matrix factorization (Margulies et al., 2016), gradients (Margulies et al., 2016), and dictionaries of functional modes (Dadi et al., 2020). What these methods have in common is the use of certain assumptions or constraints to make estimation feasible, though they differ in the specific choice of constraint. For instance, spatial ICA encourages statistical independence between network maps, leading to relatively little overlap between networks. PROFUMO and temporal ICA allow for greater spatial overlap but encourage temporal independence between networks, resulting in low FC between networks (Pervaiz et al., 2020). Relaxing these constraints, while continuing to provide sufficient model guidance for estimation accuracy and alignment of features across individuals, may permit both the temporal and spatial features of functional brain organization to be more fully expressed.

Here, we present Bayesian brain mapping (BBM), a pragmatic and flexible hierarchical Bayesian technique for producing individualized functional brain topographic maps without strong constraints on the spatial or temporal structure of the networks. BBM begins with a *template*, which can take the form of either a group parcellation or a set of continuous network maps. That template is used as the basis for population-derived priors on spatial topography and FC, which are then used to inform subject-level estimation of those same features. BBM is a generalization of template ICA (Mejia et al., 2020), which uses group ICA maps as the template, but BBM allows for parcellations, ICA maps, PROFUMO modes, and other types of network

maps as the template.

In this work, we describe BBM, illustrate its use, and provide resources to facilitate its adoption. We have three primary goals. First, we demonstrate the use of the `BayesBrainMap` R package, which includes functions to establish population-derived priors and for subject-level model fitting to derive individual functional topography and connectivity. Second, we illustrate the flexibility of BBM to work with various choices of template, including parcellations and continuous network maps, and how the priors relax the more constrained templates. Finally, we share high-quality population-derived priors for healthy young adults using data from the Human Connectome Project (HCP) (Van Essen et al., 2013). These priors can be directly adopted to apply BBM in studies of healthy young adults; for studies of different populations or to use different templates, our pipeline can be adapted to produce custom priors.

2 Methods

Figure 1 illustrates the BBM framework. The chosen template is first used to construct population-derived priors for the functional topography of and temporal synchrony between networks. These encode inherent population variability in the boundaries, configuration, and overlap of networks, effectively relaxing the constraints of the template. Training subjects from a representative population are used to derive the priors. This training set can comprise hold-out data from the focal study or data from a representative repository such as the HCP or Alzheimer’s Disease Neuroimaging Initiative (Mueller et al., 2005). The priors are in turn used to guide and inform estimation in a subject-level Bayesian model, avoiding the need to fit a large multi-subject hierarchical model. This ability to analyze data from a single subject at a time makes BBM highly pragmatic, computationally efficient, parallelizable, and clinically feasible.

The BBM population-derived priors reduce noise while retaining signal, resulting in more reliable individual-level network topography maps and the functional connectivity between them (Mejia et al., 2020, 2023, 2025). An important feature of the functional topography priors is that the population variance of each network varies across the brain, generally showing greater

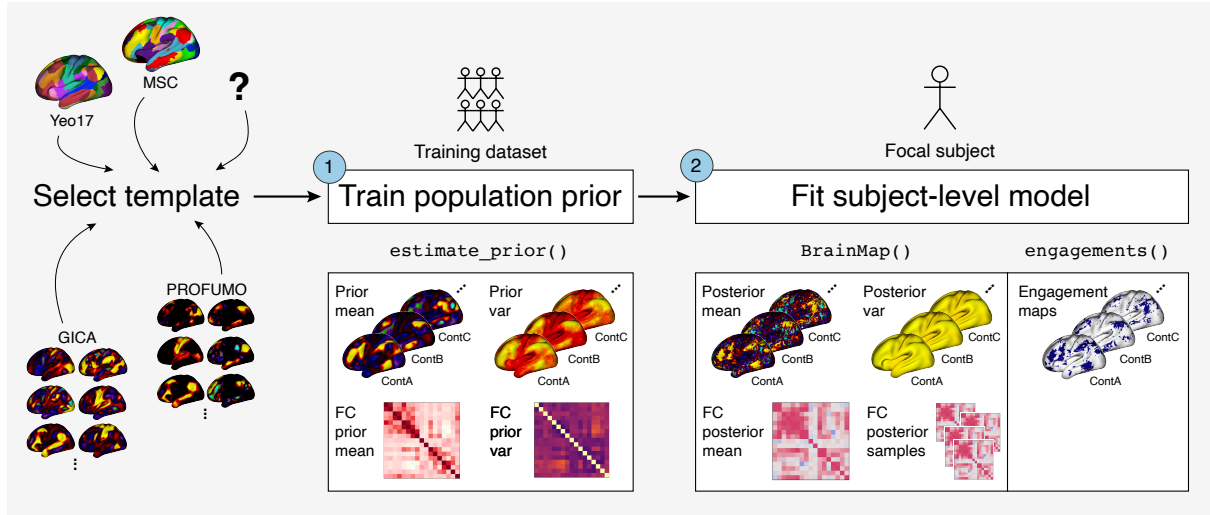


Figure 1: Overview of Bayesian Brain Mapping. The two main steps are (1) prior estimation and (2) model fitting, both implemented in the `BayesBrainMap` R package.

inter-individual differences where engagement is high, and greater similarity across subjects in background regions (Figure 1). This allows individual differences to be expressed where they exist, while reducing noise in background regions through shrinkage. Due to the continuous, whole-brain nature of BBM network maps, noise reduction in background regions of one network also indirectly contributes to estimation of signal in the same area of the brain in other networks.

The BBM model includes an optional population-derived prior on the FC between networks to encode population trends and variability in connectivity. We recently developed a novel informative prior for correlation matrices based on Cholesky factorization for this purpose (Mejia et al., 2025), which accurately captures population patterns of variability in FC. By contrast, the inverse Wishart distribution, a common choice of parametric prior for FC due to its conjugacy with the multivariate Normal distribution (Honnarat et al., 2019; Harrison et al., 2020; Mejia et al., 2025), has limited ability to model variance patterns. The BBM FC prior shrinks the subject-level FC toward the population mean to alleviate sampling error and within-subject variability, building on a long literature of the benefits of Bayesian shrinkage for FC estimation (Ledoit and Wolf, 2004; Su et al., 2009; Chen et al., 2010; Varoquaux et al., 2010; Shou et al., 2014; Mejia et al., 2015; Dai et al., 2017; Mejia et al., 2018; Rahim et al., 2019; Pervaiz et al., 2020; Honnorat and Habes, 2022).

In this section, we describe and illustrate the two main steps in BBM: prior estimation and model fitting. We first present the Bayesian model for individual-level functional topography and connectivity with population priors. We then describe how we derive the priors, illustrating the process using data from the HCP. Our HCP-derived priors are freely available for download, and we share our code so it can be adapted to other contexts. We also illustrate application of BBM to individuals from the HCP. All of the techniques described here are implemented in the `BayesBrainMap` R package, and code for the analyses presented here are available via Github.

2.1 Hierarchical Bayesian model

For a given subject and session, let y_{tv} be the preprocessed BOLD fMRI time series at location v and time point t . The BBM model assumes the BOLD time series can be linearly deconstructed into contributions from a set of networks. The model is similar to ICA and other source separation models, but without strong temporal or spatial constraints.

$$y_{tv} = \sum_{q=1}^Q a_{tq} s_{qv} + e_{tv} = \mathbf{a}_t^\top \mathbf{s}_v + e_{tv}, \quad e_{tv} \sim N(0, \tau_v^2) \quad (1)$$

$$s_{qv} = s_{qv}^0 + \delta_{qv}, \quad \delta_{qv} \sim N(0, \sigma_{qv}^2) \quad (2)$$

$$\mathbf{a}_t \sim N(\mathbf{0}, \mathbf{G}), \quad \mathbf{G} \sim p(\mathbf{G}) \quad (3)$$

At level (1) of the model, s_{qv} is the spatial engagement of network q at location v , and a_{tq} is the temporal activation of network q at time t . The vectors \mathbf{a}_t and \mathbf{s}_v combine those values across all Q networks. The scale of the residual white noise e_{tv} is allowed to vary spatially. In ICA and other blind source separation analyses of fMRI data, it is common to include additional components to capture structured noise from head motion and other sources. In BBM, these are not included in the model but are instead estimated and removed beforehand, as described in Mejia et al. (2020). In addition, we recommend the use of decomposition-based denoising like ICA-FIX (Griffanti et al., 2014) to reduce structured noise prior to model fitting.

Level (2) of the model incorporates the population-derived prior on the spatial topography in s_{qv} , where the population mean s_{qv}^0 and variance σ_{qv}^2 are considered known via the previ-

ously estimated prior, and the deviation terms δ_{qv} represent individual differences (Mejia et al., 2020). Spatial dependencies in δ_{qv} can be modeled via a multivariate spatial prior for additional accuracy and power, though at a higher computational cost (Mejia et al., 2023).

Level (3) of the model incorporates a population-derived prior on the FC between networks and is optional. This is accomplished by assuming a multivariate Normal prior on \mathbf{a}_t with mean zero and covariance \mathbf{G} , and assuming a population-derived hyperprior on \mathbf{G} (Mejia et al., 2025). Note that we constrain each column of the mixing matrix to unit variance (for identifiability, as often required in blind source separation), so $\text{Cov}(\mathbf{a}_t) \equiv \text{Cor}(\mathbf{a}_t)$. Hence, the covariance of \mathbf{a}_t represents the between-network FC, as the Pearson correlation between the time courses of each network. We provide two choices for the FC prior: the conjugate Inverse-Wishart distribution, which is used in PROFUMO (Harrison et al., 2020), or a novel Cholesky prior we developed for this model that accurately encodes patterns of population variance (Mejia et al., 2025). The conjugate prior allows for faster computation, while the Cholesky prior improves performance but is more computationally demanding, since it requires sampling from the prior. However, since the model is fit at the single-subject level, it is still fast compared with multi-subject hierarchical models, even with the Cholesky prior.

2.2 Population-derived priors

Here, we describe the construction of population-derived priors using training data from the HCP and illustrate the process via the `BayesBrainMap` R package. All steps are detailed in a demo available at <https://github.com/mandymejia/BayesianBrainMapping-priors>. The HCP-derived priors themselves are available through Open Science Framework (OSF) as described in the Github repo README. These priors can be directly utilized for application of BBM to analyze healthy young adults from the HCP or other datasets, as described in Section 2.3. We do not advise applying HCP-derived priors directly to study individuals from clearly distinct populations, such as children, the elderly, or patients. However, using the process and scripts provided, this workflow can be replicated to produce priors for other populations.

We estimate priors using several different choices of template, including parcellations and continuous network maps (Table 1). Note that whether the template is a hard parcellation or

GSR	Network Maps				Parcellations	
	GICA 15	GICA 25	GICA 50	PROFUMO 12	Yeo 17	MSC 15
With GSR	✓	✓	✓	✓	✓	✓
Without GSR	✓	✓	✓	✓	✓	✓

Table 1: Templates used for construction of HCP-derived priors available through OSF.

continuous, the priors and subject-level estimates of functional topography are always continuous. Specifically, we use the 17-network Yeo parcellation (Yeo et al., 2011), the Midnight Scan Club (MSC) group parcellation (Gordon et al., 2017), HCP-derived group ICA maps with 15 to 50 components (Smith et al., 2013), and group-level PROFUMO modes. For each template, we build priors with and without global signal regression (GSR), since whether or not to perform GSR is consequential and remains the subject of debate.

Before estimating the priors, we first select a high quality, balanced subject sample to ensure reliable and representative priors. Starting from the full HCP sample of $N = 1206$ subjects, we apply several filters to obtain the final sample for the priors. First, we exclude subjects with insufficient scan duration (< 10 min) after dropping the first 15 volumes and excluding volumes with excessive head motion, based on a lagged and filtered version of framewise displacement (FD) appropriate for multiband data (Power et al., 2019; Pham et al., 2023) with a threshold of 0.5mm. Second, we exclude any remaining related subjects. Finally, we balance sex within each age group. After applying all filters, our final sample contains approximately 350 subjects. Two sessions from each subject were then used to train the population-derived priors. Note that priors can also be trained using a single run from each training subject, as described below.

We now briefly describe the process of deriving the priors. For more details, see the Github demo that accompanies this manuscript. All of the steps for prior parameter estimation are implemented in the BayesBrainMap function `estimate_prior()`. Prior estimation requires a template (a parcellation or set of continuous network maps) and test-retest or single-session fMRI data from a set of n training subjects. If using single-session data, the scan is split down the middle to produce two pseudo sessions. For each subject and session, dual regression (Beckmann et al., 2009) is used to produce a noisy set of time courses and spatial maps. For parcellation templates, we use a modified version of dual regression: note that if network maps were binary and non-overlapping, then the first step of dual regression would produce the mean

time series within each parcel as the corresponding time series. If group parcels are misaligned to an individual, this will result in mixing signals from multiple networks. To allow for some misalignment between the subject-specific networks and the parcels, we simply compute the median rather than the mean within each parcel. The second step of dual regression then proceeds as usual, as a multiple linear regression model relating the fMRI time series at each location to the network time series to produce a map of engagement for each network. Those test-retest spatial engagement maps and time courses are then used to estimate the parameters for the topography and FC priors in the BBM model, as we now describe.

Estimation of the topography prior in level (2) of the model is straightforward. Consider a single location v and network q , we aim to estimate the population mean s_{qv}^0 and the population variance σ_{qv}^2 . Dropping the q and v subscripts momentarily, let x_{ij} be the dual regression estimate of spatial engagement for training subject i at session j . The prior mean s^0 is simply estimated as the mean over all subjects and sessions, \bar{x} . The prior variance σ^2 is estimated based on a simple measurement error model:

$$x_{ij} = z_i + e_{ij}, \quad e_{ij} \stackrel{\text{ind}}{\sim} (0, \sigma_e^2)$$

$$z_i \stackrel{\text{ind}}{\sim} (\mu, \sigma^2),$$

where z_i represent the true, noise-free spatial engagement, and the residuals e_{ij} are assumed independent of z_i . Our intended prior variance is the between-subject variance, σ^2 , while σ_e^2 represents noise levels in the dual regression maps. The variance terms in this model can be estimated using standard variance decomposition techniques or iterative estimation procedures for linear mixed effects models.

Estimation of the FC prior in level (3) of the BBM model is based on the $Q \times Q$ Pearson correlation matrices of the dual regression network time series, which represent the FC between networks. Briefly, two options for the prior are available: the inverse-Wishart, which is designed for covariance matrices and has a single parameter controlling the variance, resulting in limited flexibility to capture population variance patterns, and a novel informative prior for correlation matrices based on Cholesky factorizations, which we developed for this model. We refer the

reader to Mejia et al. (2025) for details. Our previous analyses found that both choices of prior are beneficial, but the novel permuted Cholesky prior outperforms the inverse-Wishart at identifying reliable FC patterns in individuals (Mejia et al., 2025).

A large training sample from a publicly available resource like the HCP is ideal for prior estimation. However, it is sometimes desirable to build a customized prior for the specific population or context of a given study. In that case, it is possible to use a holdout set which has been done successfully in previous studies (Gaddis et al., 2022; Derman et al., 2025; Butler et al., 2025). This holdout set should be large enough to accurately estimate prior parameters, ideally 100 or more, or at least several dozen. It is also possible to use the same subjects for prior estimation and subsequent subject-level analysis, an approach known as empirical Bayes (EB). While EB comes with a risk of overfitting, it also allows for using all of the available data for training, generally resulting in more accurate priors, which may be considered worth the tradeoff. It is important to visually inspect the prior mean and variance maps to assess the level of noise present in the priors. Besides a large training sample, avoiding over-processing of the training data can also reduce noise levels in the priors. Strategies to avoid over-processing include using lenient or data-driven volume censoring, parsimonious nuisance regression/denoising, and high-pass instead of band-pass filtering.

2.3 Fitting the BBM model to single-subject data

Once the priors have been estimated, the BBM model can be fit for a single individual, using a single or multiple fMRI sessions, to estimate topography and connectivity. Model fitting is implemented in the BayesBrainMap function `BrainMap()` through an iterative procedure based on expectation-maximization (Mejia et al., 2020, 2023) or variational Bayes (Mejia et al., 2025), depending on the specific model. This function produces point estimates (i.e., posterior means) of the subject-specific spatial maps and FC matrices, as well as measures of uncertainty (i.e., posterior variances) to facilitate inference.

Finally, areas of significant engagement for each network are identified based on posterior inference using the function `engagements()`. Because the BBM framework has relatively high power to detect non-zero engagements, we can specify a minimum effect size of interest for inference.

Since the spatial maps are in arbitrary units, we draw inspiration from a common method for thresholding group ICA maps, where values over z standard deviations above the mean are commonly displayed, while values below this are considered negligible and suppressed. Following this logic, we set a minimum effect size for inference as the prior mean value corresponding to z standard deviations above the mean. The `engagements()` function allows the user to specify z , or to provide multiple values for z to produce a nested set of significant engagements of different strengths (illustrated in Figure 5).

In the Github demo that accompanies this manuscript, we illustrate the use of the `BrainMap()` and `engagements()` functions to analyze several individual participants from the HCP.

3 Results

Spatial topography prior means for several components from the Yeo17 template are shown in Figure 2. While the template is constrained to have no overlap between networks, the prior relaxes that constraint. The patterns seen in the prior mean maps reflects the engagement of the network in the training sample, with no constraint to encourage or enforce spatial independence. This additional flexibility leads to expansion of the template networks beyond their original boundaries, suggesting the presence of regions that engage in multiple networks as well as population heterogeneity in the precise localization of networks.

Arrows indicate areas that differ markedly between the parcels and the prior mean maps. For instance, in the Default A network, bilateral, roughly symmetric temporal lobe engagement is seen in the prior, whereas the parcel only includes temporal lobe engagement within the right hemisphere. Another noteworthy example is engagement of Broca's area and other areas commonly associated with language in the temporal parietal network, while the corresponding parcel is constrained to the temporal lobe. Similar patterns are often seen in networks characterized by strong engagement in the superior temporal gyrus and the temporal parietal junction when using ICA or other network estimation methods that allow for overlap between networks.

The pairwise spatial overlap between networks for different templates and their corresponding priors is shown in Appendix Figure 6. Overlap is quantified using the Dice coefficient. For

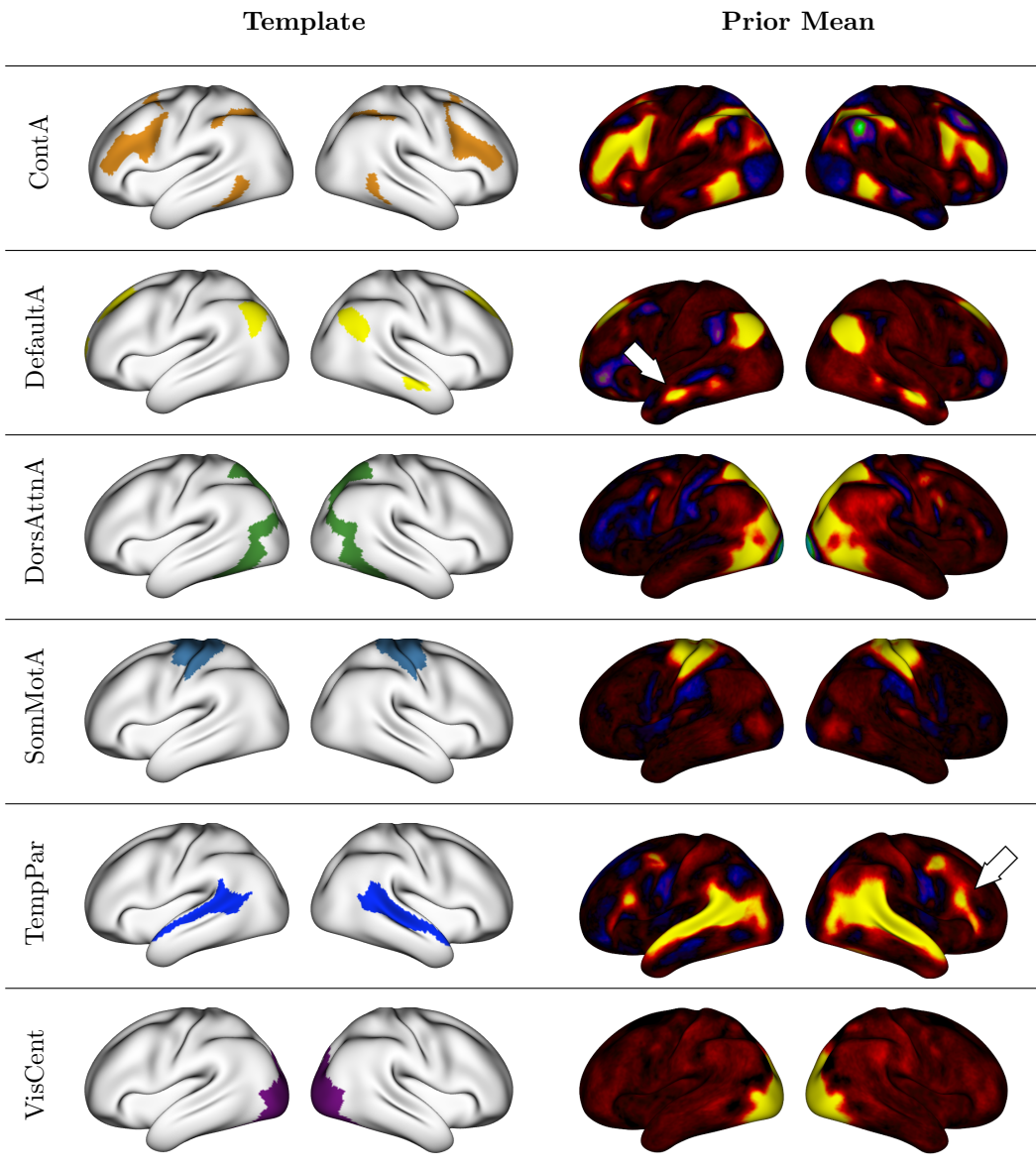


Figure 2: HCP-derived spatial topography priors for Yeo17 template. Six exemplar networks are shown. While the parcels are constrained to have no overlap, the prior mean maps for each network show expansion beyond the parcel boundaries, indicating overlapping network engagement.

continuous network maps, we first threshold the maps at a z-score of ± 2 , following a common practice for thresholding group ICA maps to isolate areas of engagement. The parcellation-based templates by definition have zero overlap between networks, but their corresponding priors exhibit overlap between certain networks. Network maps based on PROFUMO exhibit the most overlap, reflecting a key feature of PROFUMO, and the degree of overlap is similar in the template and the prior. To a slightly lesser degree, the GICA template and prior also exhibit overlap, contradicting a common belief that ICA does not allow for spatial overlap. Spatial ICA components are optimized to maximize statistical independence, which does not imply non-overlap. On the contrary, non-overlap implies anti-correlation (or from probability, disjoint events are never independent).

Spatial topography priors for a default mode network component from various templates are shown in Figure 3. Similar features are seen across the different priors, even though the templates are based on distinct model assumptions. The prior standard deviation maps show that individual variation in engagement is greatest in areas of high average engagement, reflecting differences in the configuration, size, and distribution of networks across individuals. The low prior variance in background areas, where true population variability is low, will result in a high degree of regularization in these areas for the corresponding networks. Higher prior variance in areas of engagement, by contrast, will allow for individual features to be expressed. Furthermore, due to the additive nature of the decomposition, noise reduction in background areas of certain networks will indirectly improve estimation of engagement in other networks corresponding to the same physical location.

The functional connectivity priors in BBM are illustrated in Figure 4 for the Yeo17 template and in Appendix Figure 7 for other templates. The element-wise empirical mean and standard deviation within the training set, representing population tendencies and variability, are shown in the first column. The second two columns show the corresponding values based on the two choices of FC prior in BBM: the permuted Cholesky prior described in Mejia et al. (2025) and the conjugate inverse Wishart (IW). While both priors capture the population mean, only the Cholesky prior accurately captures the population variance. This is because the IW distribution for covariance matrices includes a single scalar parameter that moderates the variance across the matrix, so that the element-wise variance is monotonically related to the element-wise mean.

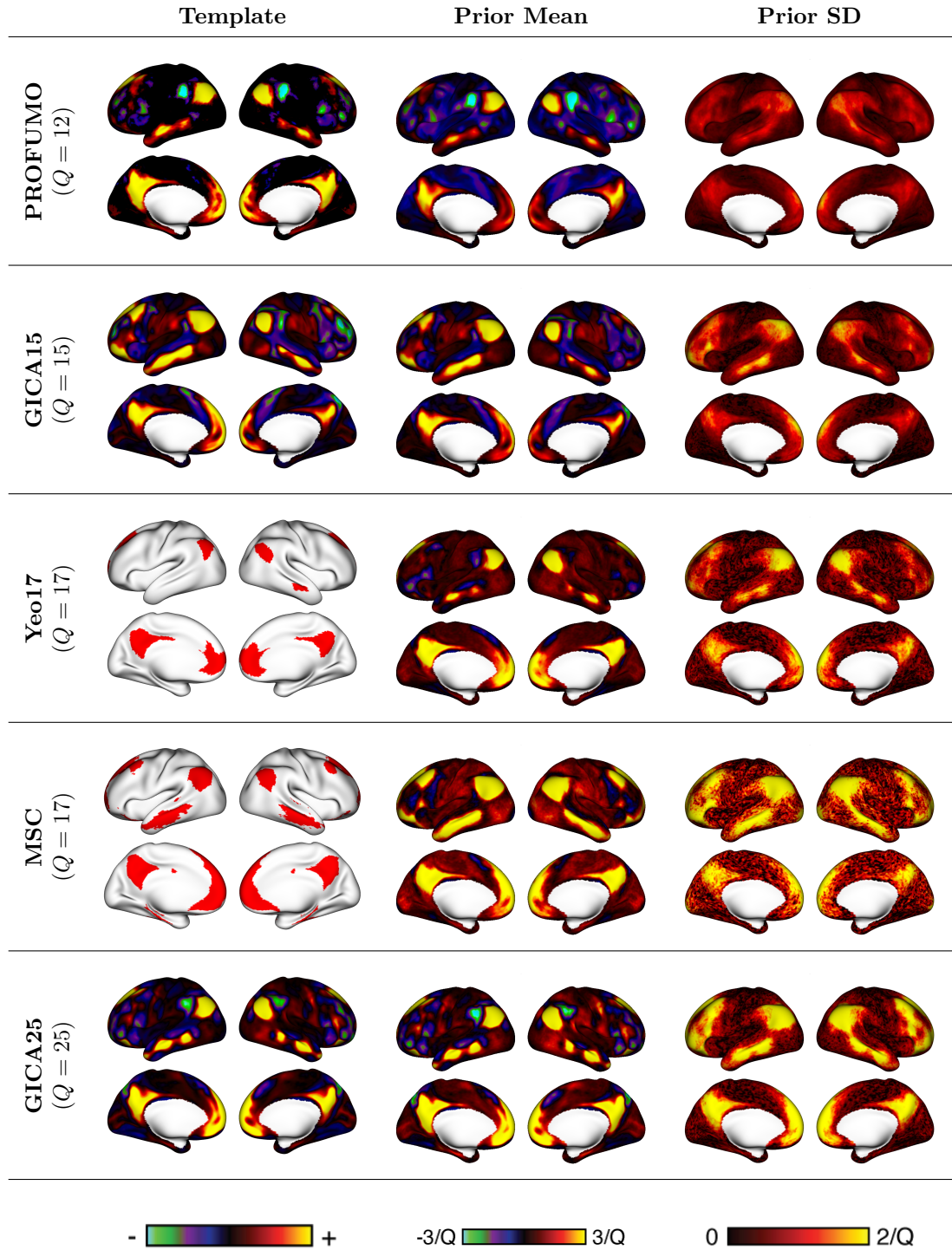


Figure 3: HCP-derived spatial topography priors for a default mode network component from various templates. Templates include two parcellations (Yeo17 and MSC) and two types of network maps (ICA and PROFUMO) and are ordered from lowest to highest resolution (number of networks). The specific networks displayed are PROFUMO mode 8, GICA15 component 2, Yeo17 Default A, MSC Default, and GICA25 IC 2. Template maps are displayed on an arbitrary scale, while the scale of the priors is inversely proportional to the template resolution Q , given the additive nature of the BBM decomposition.

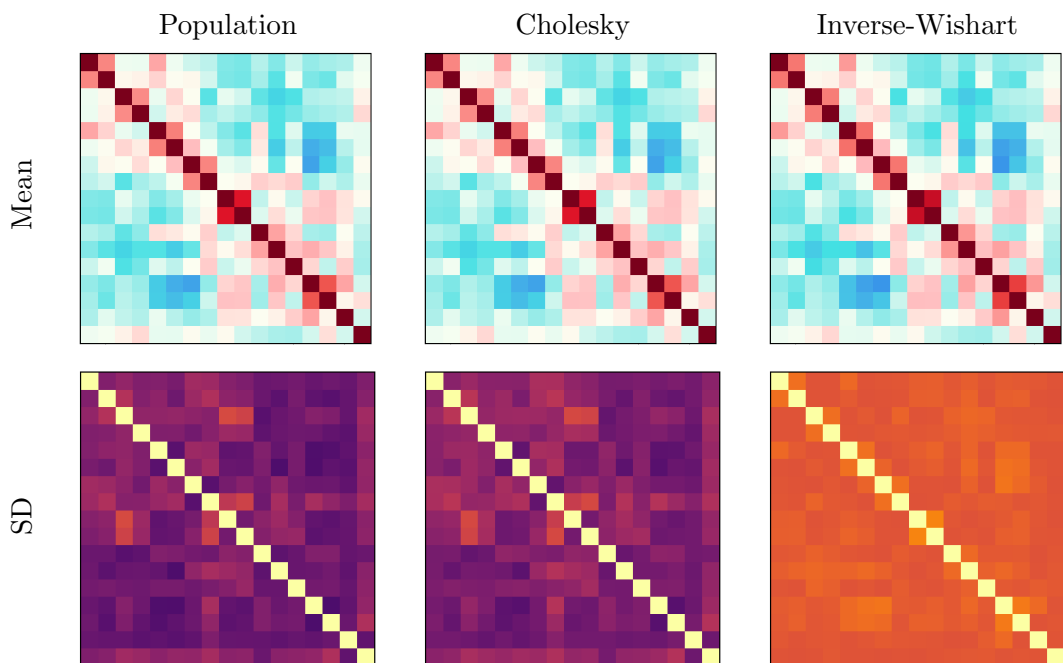


Figure 4: Example of the functional connectivity (FC) prior in BBM, based on the Yeo17 template. The element-wise empirical mean and standard deviation (SD) within the training set used to establish the priors are show in the first column. The second and third columns show the element-wise mean and SD based on the Cholesky and the inverse Wishart choices of prior. The population mean is captured by both priors, but only the Cholesky prior captures the population variance patterns.

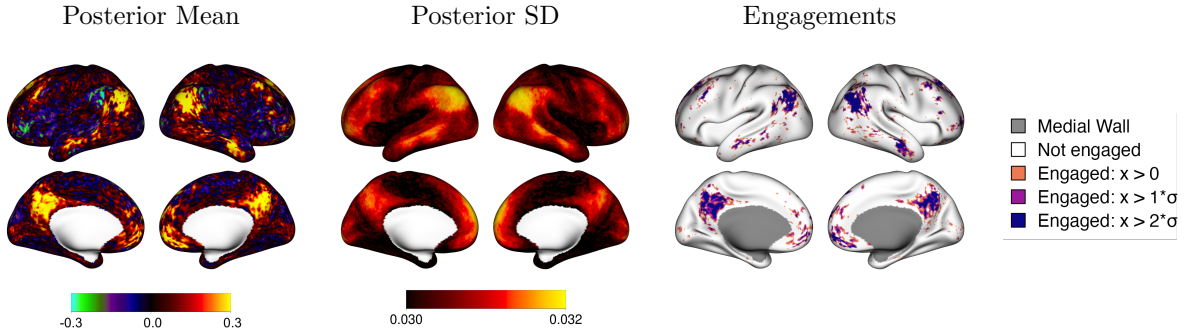


Figure 5: Example individual BBM spatial engagement maps. A single HCP subject was analyzed using BBM with population-derived priors based on the Yeo17 template. The BBM posterior mean and standard deviation for a network corresponding to the Yeo17 DefaultA parcel are shown, along with areas of statistically significant engagement. Significance is based on the Bayesian equivalent of a hypothesis test with $\alpha = 0.05$ and Bonferroni correction. A range of effect size thresholds are specified based on σ , the standard deviation of the prior mean map. This is analogous to the common practice of thresholding group ICA maps at a certain number of standard deviations from the mean to isolate the main areas of engagement.

In BBM, this parameter is chosen to minimize the difference between the population and prior element-wise variance, but with a constraint that the prior variance should not be less than the population variance anywhere. This avoids an overly informative prior, which would result in too much shrinkage towards the group and loss of relevant individual information. Due to this limitation of the inverse Wishart distribution, the IW FC prior tends to have much higher variance for many FC edges compared with the population, resulting in weak shrinkage. The Cholesky prior, by contrast, is more informative while not being overly informative, which serves to maximize accuracy of FC estimates, and has indeed been shown to produce more reliable and individualized estimates of between-network FC (Mejia et al., 2025). Improved estimation of the temporal component of the BBM model may also have downstream benefits for estimation of spatial topography, since the temporal and spatial components are estimated iteratively.

Figure 5 shows example individual-level spatial topography maps produced by applying BBM to analyze data from one HCP subject, using population-derived priors based on the Yeo17 template. A single network is shown corresponding to the DefaultA parcel. The posterior mean provides an estimate of engagement in the network at every vertex, while the posterior standard deviation represents uncertainty around that estimate. Binary maps of statistically significant engagement are produced based on the posterior mean and standard deviation, using the Bayesian equivalent of a hypothesis test. A range of minimum effect sizes are tested against,

resulting in nested sets of significantly engaged vertices. The ability to specify a minimum effect size gives the researcher flexibility to focus on locations that exhibit intense network engagement, or to consider all vertices that exhibit engagement that is significantly different from zero. The researcher can also consider a range of minimum effect sizes, as we have done here, to distinguish between levels of engagement.

4 Discussion

In this paper we illustrate Bayesian brain mapping (BBM), a source separation technique for fMRI that leverages population information through population-derived priors to reliably estimate individual-level network topography and functional connectivity. Those priors use established network maps, such as parcellations or group ICA maps, as templates, producing individual-specific analogues of known networks. The priors relax constraints of the template, allowing for overlap between networks and differential engagement within networks. The powerful noise reduction properties of the priors facilitate reliable estimation of individualized functional topography with moderate scan duration, mitigating the need for extensive scanning of individuals. We also provide resources to facilitate its implementation, including a demo illustrating the BayesBrainMap R package functions for prior estimation, model fitting, and inference, as well as HCP-derived priors based on a range of templates.

Several areas of future work are planned to extend BBM to a wider variety of settings and introduce new capabilities. These include transfer learning to adapt priors to new populations without large training samples, algorithms for computationally efficient spatial modeling to enhance accuracy and power, inclusion of covariates and nuisance effects such as site and scanner, and mixture priors for heterogeneous populations. All extensions will be implemented in BayesBrainMap as they are developed.

References

Beckmann, C. F., Mackay, C. E., Filippini, N., and Smith, S. M. (2009). Group comparison of resting-state fMRI data using multi-subject ICA and dual regression. *Neuroimage*, 47(Suppl

1):S148.

Beckmann, C. F. and Smith, S. M. (2004). Probabilistic independent component analysis for functional magnetic resonance imaging. *IEEE transactions on medical imaging*, 23(2):137–152.

Bijsterbosch, J., Woolrich, M., Glasser, M., Robinson, E., Beckmann, C., Van Essen, D., Harrison, S., and Smith, S. (2018). The relationship between spatial configuration and functional connectivity of brain regions. *eLife*, 7:e32992.

Bijsterbosch, J. D., Beckmann, C. F., Woolrich, M. W., Smith, S. M., and Harrison, S. J. (2019). The relationship between spatial configuration and functional connectivity of brain regions revisited. *Elife*, 8:e44890.

Bijsterbosch, J. D., Farahibozorg, S.-R., Glasser, M. F., Van Essen, D., Snyder, L. H., Woolrich, M. W., and Smith, S. M. (2023). Evaluating functional brain organization in individuals and identifying contributions to network overlap. *Imaging Neuroscience*, 1:1–19.

Braga, R. M. and Buckner, R. L. (2017). Parallel interdigitated distributed networks within the individual estimated by intrinsic functional connectivity. *Neuron*, 95(2):457–471.

Butler, E. R., Samia, N. I., Mejia, A. F., Pham, D. D., Pines, A., and Nusslock, R. (2025). Sex differences in response to violence: role of salience network expansion and connectivity on depression. *Translational Psychiatry*, 15(1):427.

Chen, Y., Wiesel, A., Eldar, Y. C., and Hero, A. O. (2010). Shrinkage algorithms for mmse covariance estimation. *IEEE transactions on signal processing*, 58(10):5016–5029.

Dadi, K., Varoquaux, G., Machlouzarides-Shalit, A., Gorgolewski, K. J., Wassermann, D., Thirion, B., and Mensch, A. (2020). Fine-grain atlases of functional modes for fmri analysis. *NeuroImage*, 221:117126.

Dai, T., Guo, Y., Initiative, A. D. N., et al. (2017). Predicting individual brain functional connectivity using a bayesian hierarchical model. *NeuroImage*, 147:772–787.

Derman, D., Pham, D. D., Mejia, A. F., and Ferradal, S. L. (2025). Individual patterns of functional connectivity in neonates as revealed by surface-based Bayesian modeling. *Imaging Neuroscience*, 3:imag.a.00504.

Farahibozorg, S.-R., Bijsterbosch, J. D., Gong, W., Jbabdi, S., Smith, S. M., Harrison, S. J., and Woolrich, M. W. (2021). Hierarchical modelling of functional brain networks in population and individuals from big fMRI data. *NeuroImage*, 243:118513.

Faskowitz, J., Esfahlani, F. Z., Jo, Y., Sporns, O., and Betzel, R. F. (2020). Edge-centric functional network representations of human cerebral cortex reveal overlapping system-level architecture. *Nature neuroscience*, 23(12):1644–1654.

Finn, E. S., Shen, X., Scheinost, D., Rosenberg, M. D., Huang, J., Chun, M. M., Papademetris, X., and Constable, R. T. (2015). Functional connectome fingerprinting: identifying individuals using patterns of brain connectivity. *Nature neuroscience*, 18(11):1664–1671.

Gaddis, A., Lidstone, D., Nebel, M., Griffiths, R., Mostofsky, S., Mejia, A., and Barrett, F. (2022). Psilocybin induces spatially constrained alterations in thalamic functional organization and connectivity. *Neuroimage*, 260:119434.

Gordon, E. M., Laumann, T. O., Gilmore, A. W., Newbold, D. J., Greene, D. J., Berg, J. J., Ortega, M., Hoyt-Drazen, C., Gratton, C., Sun, H., et al. (2017). Precision functional mapping of individual human brains. *Neuron*, 95(4):791–807.

Griffanti, L., Salimi-Khorshidi, G., Beckmann, C. F., Auerbach, E. J., Douaud, G., Sexton, C. E., Zsoldos, E., Ebmeier, K. P., Filippini, N., Mackay, C. E., et al. (2014). ICA-based artefact removal and accelerated fMRI acquisition for improved resting state network imaging. *Neuroimage*, 95:232–247.

Guo, Y. and Tang, L. (2013). A hierarchical model for probabilistic independent component analysis of multi-subject fMRI studies. *Biometrics*, 69(4):970–981.

Harrison, S. J., Bijsterbosch, J. D., Segerdahl, A. R., Fitzgibbon, S. P., Farahibozorg, S.-R., Duff, E. P., Smith, S. M., and Woolrich, M. W. (2020). Modelling subject variability in the spatial and temporal characteristics of functional modes. *NeuroImage*, 222:117226.

Harrison, S. J., Woolrich, M. W., Robinson, E. C., Glasser, M. F., Beckmann, C. F., Jenkinson, M., and Smith, S. M. (2015). Large-scale probabilistic functional modes from resting state fmri. *NeuroImage*, 109:217–231.

Honnorat, N., Adeli, E., Zhao, Q., Pfefferbaum, A., Sullivan, E. V., and Pohl, K. (2019). Covariance shrinkage for dynamic functional connectivity. In *International Workshop on Connectomics in Neuroimaging*, pages 32–41. Springer.

Honnorat, N. and Habes, M. (2022). Covariance shrinkage can assess and improve functional connectomes. *NeuroImage*, 256:119229.

Kong, R., Li, J., Orban, C., Sabuncu, M. R., Liu, H., Schaefer, A., Sun, N., Zuo, X.-N., Holmes, A. J., Eickhoff, S. B., et al. (2019). Spatial topography of individual-specific cortical networks predicts human cognition, personality, and emotion. *Cerebral cortex*, 29(6):2533–2551.

Kong, R., Yang, Q., Gordon, E., Xue, A., Yan, X., Orban, C., Zuo, X.-N., Spreng, N., Ge, T., Holmes, A., et al. (2021). Individual-specific areal-level parcellations improve functional connectivity prediction of behavior. *Cerebral Cortex*, 31(10):4477–4500.

Ledoit, O. and Wolf, M. (2004). A well-conditioned estimator for large-dimensional covariance matrices. *Journal of multivariate analysis*, 88(2):365–411.

Li, X., Gan, J. Q., and Wang, H. (2018). Collective sparse symmetric non-negative matrix factorization for identifying overlapping communities in resting-state brain functional networks. *NeuroImage*, 166:259–275.

Li, Y., Liu, A., Fu, X., McKeown, M. J., Wang, Z. J., and Chen, X. (2022). Atlas-guided parcellation: Individualized functionally-homogenous parcellation in cerebral cortex. *Computers in Biology and Medicine*, 150:106078.

Margulies, D. S., Ghosh, S. S., Goulas, A., Falkiewicz, M., Huntenburg, J. M., Langs, G., Bezgin, G., Eickhoff, S. B., Castellanos, F. X., Petrides, M., et al. (2016). Situating the default-mode network along a principal gradient of macroscale cortical organization. *Proceedings of the National Academy of Sciences*, 113(44):12574–12579.

Mejia, A. F., Bolin, D., Spencer, D. A., and Eloyan, A. (2025). Leveraging population information in brain connectivity via bayesian ica with a novel informative prior for correlation matrices. *Biostatistics*, 26(1):kxaf022.

Mejia, A. F., Bolin, D., Yue, Y. R., Wang, J., Caffo, B. S., and Nebel, M. B. (2023). Template independent component analysis with spatial priors for accurate subject-level brain network estimation and inference. *Journal of Computational and Graphical Statistics*, 32(2):413–433.

Mejia, A. F., Nebel, M. B., Barber, A. D., Choe, A. S., Pekar, J. J., Caffo, B. S., and Lindquist, M. A. (2018). Improved estimation of subject-level functional connectivity using full and partial correlation with empirical bayes shrinkage. *NeuroImage*, 172:478–491.

Mejia, A. F., Nebel, M. B., Shou, H., Crainiceanu, C. M., Pekar, J. J., Mostofsky, S., Caffo, B., and Lindquist, M. A. (2015). Improving reliability of subject-level resting-state fmri parcellation with shrinkage estimators. *NeuroImage*, 112:14–29.

Mejia, A. F., Nebel, M. B., Wang, Y., Caffo, B. S., and Guo, Y. (2020). Template independent component analysis: Targeted and reliable estimation of subject-level brain networks using big data population priors. *Journal of the American Statistical Association*, 115(531):1151–1177.

Mueller, S. G., Weiner, M. W., Thal, L. J., Petersen, R. C., Jack, C., Jagust, W., Trojanowski, J. Q., Toga, A. W., and Beckett, L. (2005). The alzheimer’s disease neuroimaging initiative. *Neuroimaging Clinics*, 15(4):869–877.

Pervaiz, U., Vidaurre, D., Woolrich, M. W., and Smith, S. M. (2020). Optimising network modelling methods for fmri. *NeuroImage*, 211:116604.

Pham, D. D., McDonald, D. J., Ding, L., Nebel, M. B., and Mejia, A. F. (2023). Less is more: balancing noise reduction and data retention in fmri with data-driven scrubbing. *NeuroImage*, 270:119972.

Power, J. D., Lynch, C. J., Silver, B. M., Dubin, M. J., Martin, A., and Jones, R. M. (2019). Distinctions among real and apparent respiratory motions in human fmri data. *NeuroImage*, 201:116041.

Rahim, M., Thirion, B., and Varoquaux, G. (2019). Population shrinkage of covariance (posce) for better individual brain functional-connectivity estimation. *Medical image analysis*, 54:138–148.

Shou, H., Eloyan, A., Nebel, M. B., Mejia, A., Pekar, J. J., Mostofsky, S., Caffo, B., Lindquist, M. A., and Crainiceanu, C. M. (2014). Shrinkage prediction of seed-voxel brain connectivity using resting state fmri. *NeuroImage*, 102:938–944.

Smith, S. M., Miller, K. L., Moeller, S., Xu, J., Auerbach, E. J., Woolrich, M. W., Beckmann, C. F., Jenkinson, M., Andersson, J., Glasser, M. F., et al. (2012). Temporally-independent functional modes of spontaneous brain activity. *Proceedings of the National Academy of Sciences*, 109(8):3131–3136.

Smith, S. M., Miller, K. L., Salimi-Khorshidi, G., Webster, M., Beckmann, C. F., Nichols, T. E., Ramsey, J. D., and Woolrich, M. W. (2011). Network modelling methods for fmri. *Neuroimage*, 54(2):875–891.

Smith, S. M., Vidaurre, D., Beckmann, C. F., Glasser, M. F., Jenkinson, M., Miller, K. L., Nichols, T. E., Robinson, E. C., Salimi-Khorshidi, G., Woolrich, M. W., et al. (2013). Functional connectomics from resting-state fmri. *Trends in cognitive sciences*, 17(12):666–682.

Su, S.-C., Caffo, B., Garrett-Mayer, E., and Bassett, S. S. (2009). Modified test statistics by inter-voxel variance shrinkage with an application to f mri. *Biostatistics*, 10(2):219–227.

Van Essen, D. C., Smith, S. M., Barch, D. M., Behrens, T. E., Yacoub, E., Ugurbil, K., Consortium, W.-M. H., et al. (2013). The wu-minn human connectome project: an overview. *Neuroimage*, 80:62–79.

Varoquaux, G., Gramfort, A., Poline, J.-B., and Thirion, B. (2010). Brain covariance selection: better individual functional connectivity models using population prior. *Advances in neural information processing systems*, 23.

Xue, A., Kong, R., Yang, Q., Eldaief, M. C., Angeli, P. A., DiNicola, L. M., Braga, R. M., Buckner, R. L., and Yeo, B. T. (2021). The detailed organization of the human cerebellum estimated by intrinsic functional connectivity within the individual. *Journal of neurophysiology*, 125(2):358–384.

Yeo, B. T., Krienen, F. M., Sepulcre, J., Sabuncu, M. R., Lashkari, D., Hollinshead, M., Roffman, J. L., Smoller, J. W., Zöllei, L., Polimeni, J. R., et al. (2011). The organization of the human cerebral cortex estimated by intrinsic functional connectivity. *Journal of neurophysiology*.

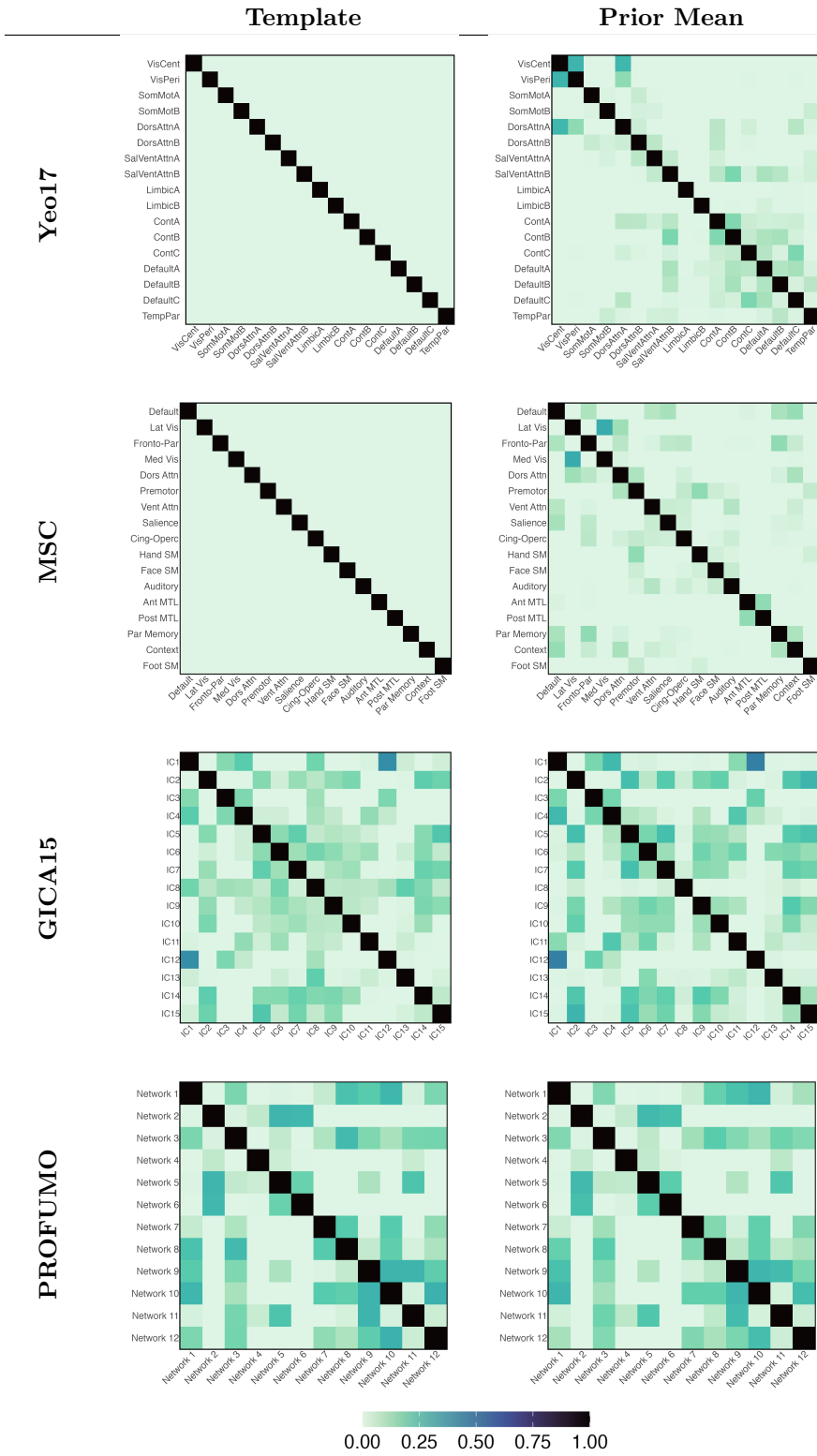


Figure 6: Dice overlap matrices comparing each template with its prior mean. Yeo17 and MSC used hard labels; GICA and PROFUMO maps were thresholded at $|z| \geq 2$.

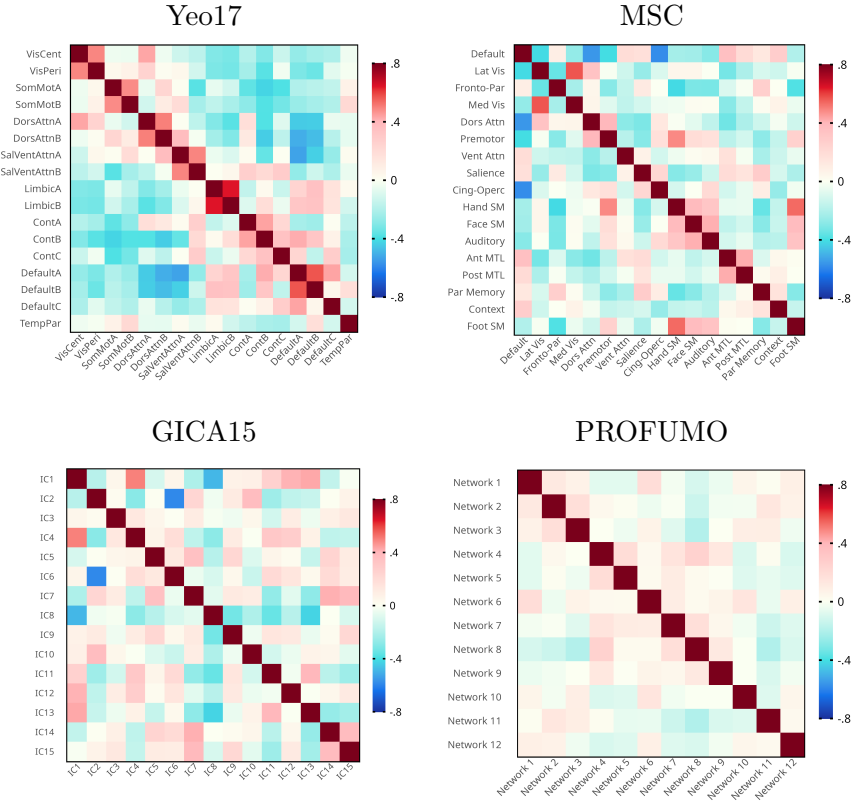


Figure 7: Functional connectivity priors for various templates. The empirical element-wise population mean of FC across the prior training sample is shown. The empirical population mean and variance are not used directly in the BBM model. Rather, the Inverse-Wishart or permuted Cholesky prior is built based on the FC training samples.